THE JOURNAL OF PHYSICAL CHEMISTRY C
A JOURNAL OF THE AMERICAN CHEMICAL SOCIETY

pubs.acs.org/JPCC

Article

Impact of Chemical Primers on the Growth, Structure, and Functional Properties of ZIF-8 Films

Juan A. Allegretto,* Melina Arcidiácono, Paula Y. Steinberg, Paula C. Angelomé, Omar Azzaroni, and Matias Rafti*

Cite This: *J. Phys. Chem. C* 2022, 126, 6724−6735

Read Online

ACCESS | Metrics & More | Article Recommendations | Supporting Information

ABSTRACT: ZIF-8 (zeolitic imidazolate framework) metal−organic framework (MOF) thin films have been studied extensively given their possible applications in separation membranes and sensors and even for microelectronics. The wide variety of substrates and synthetic strategies used for ZIF-8 film formation causes a dispersion in the properties observed, and elucidation of the influence of each step in such processes is a much-desired goal that remains partially unexplored. Therefore, we herein focused on a thorough characterization of the effect of substrate surface chemistry given by chemical primers on the resulting films. Specifically, we used self-assembled monolayers (SAMs) of 3-mercapto-1-propanesulfonic acid (MPSA) and (3-aminopropyl)triethoxysilane (APTES). We have analyzed and evaluated its influence on growth progression, thickness, crystallinity, surface roughness, compactness, and porosity on ZIF-8 films grown via a one-pot liquid-phase epitaxy approach and the overall impact of those properties on molecular transport of different probes. We observed significant differences regarding transport properties, and thus available porosity, even for films featuring similar thickness, a parameter widely employed for film comparison. While MPSA renders more compact films and permselectivity, the same synthesis procedure applied to APTES-primed substrates yields lower compactness and lower selectivity on molecular transport. Altogether, our results demonstrate that surface chemical modification of substrates plays a fundamental role in the resulting MOF film structure and thus can be used to modulate crucial properties for prospective use in technological devices.

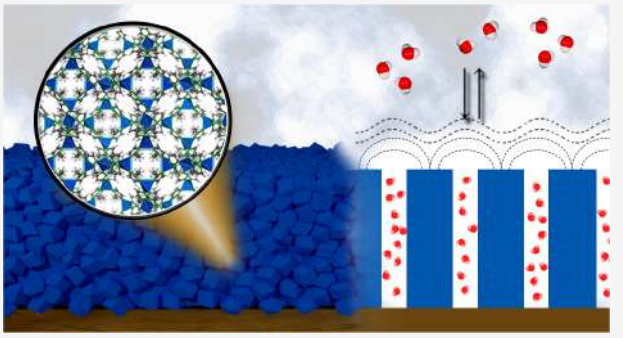

INTRODUCTION

Since the advent of metal−organic frameworks (MOFs),[1,2] an ever-increasing number of reports deal with their versatility in terms of crystalline structure and morphology,[3] surface chemistry, functional properties, and potential for integration into diverse platforms.[4,5] Furthermore, this activity stimulated an extended quest for further applications in diverse fields.[6−8] A particularly interesting approach enabling many applications is to synthesize MOFs in a film configuration, which allows one to acquire detailed control over surface and interfacial properties. Over the past few years, several reviews have been published covering various aspects of MOF films synthesis and their potential applications in energy, separations, or sensing, just to name a few prominent examples.[9−12]

One way of achieving continuous, crystalline, and smooth MOF films is to modify the substrate employed with a suitable primer, which should ideally expose appropriate chemical moieties to boost MOF heterogeneous nucleation. Having created such a primer structure, it is possible then to grow films by alternatively exposing substrates to solutions of the linker and metallic ion, a procedure known as step-by-step liquid-phase epitaxy (LPE), which can lead to the formation of films known as surface-attached MOFs or SURMOFs.[13−15] SURMOFs allow the fine-tuning of film thickness as well as further control over crystalline orientation. Another advantage of using highly oriented crystalline SURMOFs is the minimization (or even suppression) of diffusion barriers, which decrease mass transfer and thus affect separation performance.[16] Although thickness for SURMOFs is usually defined up to a few tens of nanometers, there are few reports of relatively thick SURMOFs (70−100 nm).[17−19] Thicker films can be also obtained by using a modified LPE procedure in which a one-pot direct mix of precursors is carried; in this way, synthesis time can be reduced, although the payoff is some degree of control loss regarding film structure. It is evident then, the importance of understanding synthetic approaches in order to produce continuous and relatively thick MOF films in a controlled and reproducible fashion, with high reproduci-

Received: December 9, 2021
Revised: February 17, 2022
Published: April 6, 2022

https://doi.org/10.1021/acs.jpcc.1c10425
J. Phys. Chem. C 2022, 126, 6724−6735

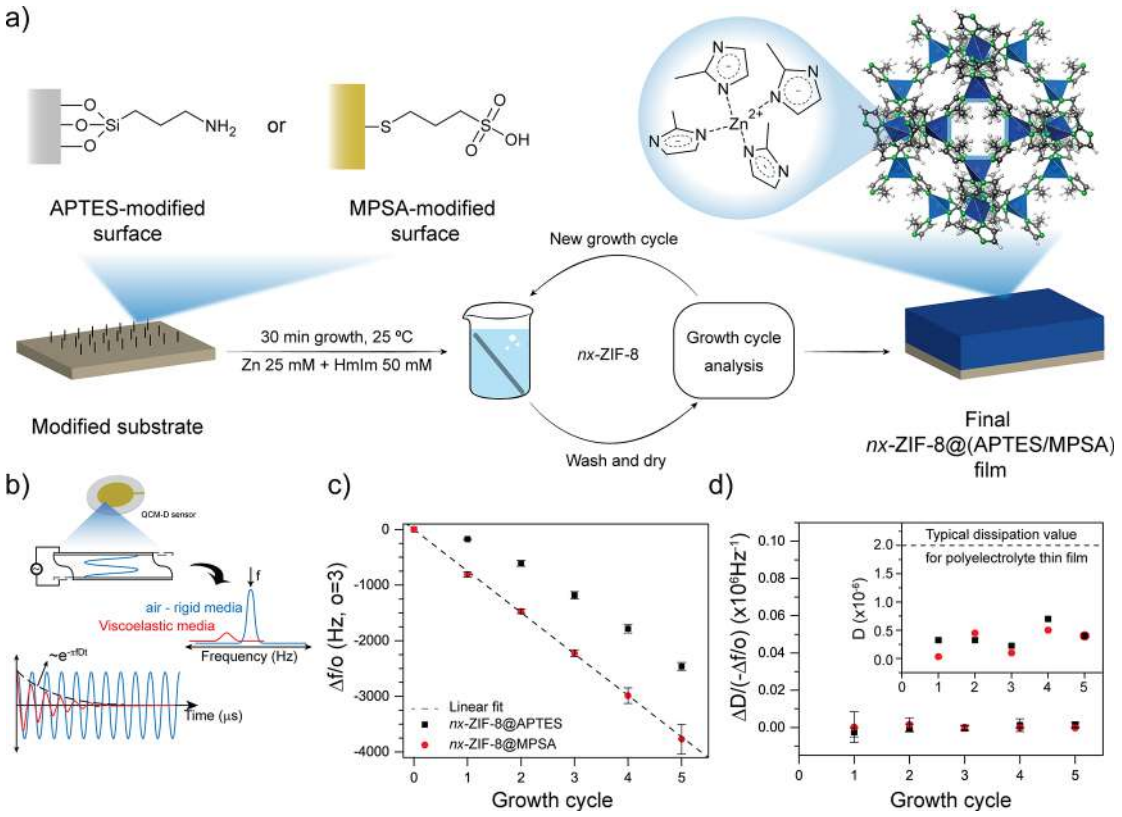

Figure 1. (a) Scheme for surface modification and procedure followed for ZIF-8 film growth. (b) Scheme of QCM-D fundamentals in rigid and viscoelastic media. Changes in (c) frequency (dashed: linear fit) and (d) dissipation factor normalized by frequency change after each ZIF-8 growth cycle. (d, inset) Absolute dissipation factor change. o: overtone. Error bars: Standard deviation of the mean.

bility regarding key functional features such as thickness, coverage, and porosity.

For a certain material to be considered as a prospect toward a given application, it must fulfill basic requirements regarding structural stability upon exposure to relevant working conditions (e.g., solvent, pH, temperature, ionic strength). Zeolitic imidazolate frameworks (ZIF-MOFs) in general, and zinc/2-methylimidazole-based ZIF-8 in particular, constitute a particularly interesting example of a porous material due to its ability to meet such criteria. ZIF-8 stands out due to its inherent hydrophobic microporosity (1.16 nm pore diameter with 0.34 nm pore aperture, and BET surface areas up to 1600 $m^2\ g^{-1}$), with relatively high chemical and thermal stability.[20−22] There are various recently reported interesting examples dealing with potential applications of ZIF-8 films including gas- and liquid-phase separations,[23,24] sensing,[25,26] catalysis,[27,28] and electrocatalysis.[29−31]

Any intended improvement regarding approaches to efficient and controlled synthesis of ZIF-8 films relies necessarily upon a thorough understanding of the growth process (specifically during one-pot LPE synthesis) and the influence of substrate surface chemistry. Aside from procedures omitting a primer,[32−34] or the recently proposed use of polymeric brushes as 3D primers,[35−37] most traditional approaches make use of 2D primers such as silanes layers and thiol self-assembled monolayers (SAMs). The choice of one layer or another relies on the final purpose of the film. For instance, silanes allow the modification of silicon, glass, and nonmetallic conductive substrates (e.g., indium tin oxide (ITO) coated glass), and even capillary tubes.[38−40] On the other hand, thiols allow the functionalization of metal surfaces in an ordered fashion whose plasmonic and conductive properties to be exploited.[17,41−45] One particular point that cannot be omitted, is the influence of the density of nucleation points across the substrate's surface and how this can potentially affect the heterogeneous nucleation of films.[37,42] Furthermore, when films grown on different substrates are analyzed, the resulting variation in surface chemistry, density and distribution of nucleation points, and synthesis conditions make comparison among them a very challenging task.

Herein, we tackle this problem by performing a direct comparison on the effect of nucleation points on the growth of ZIF-8 films by comparing films grown via consecutive one-pot LPE on two model substrate surfaces exposing primary amine and sulfonic acid moieties, namely, (3-aminopropyl)-triethoxysilane or APTES, and 3-mercapto-1-propanesulfonic acid or MPSA. The comparison is based on a characterization of growth dynamics, structure (both morphology and crystallinity), and porosity. To this end, quartz-crystal microbalance with dissipation monitoring (QCM-D) and spectroscopic ellipsometry experiments were carried out to characterize the thickness evolution (results were also compared with previous reports using optical waveguide spectroscopy (OWS)). Structural characterization was conducted by X-ray diffraction (XRD) and X-ray reflectivity (XRR), while atomic force microscopy (AFM) and X-ray photoelectron spectroscopy (XPS) were employed for characterization of morphology and surface chemistry. Finally, functional properties related to permeability, in terms of molecular transport of redox probes through a film's porosity, were probed via cyclic voltammetry,[43,44,46,47] and the obtained

https://doi.org/10.1021/acs.jpcc.1c10425
J. Phys. Chem. C 2022, 126, 6724−6735

results were analyzed using the partially blocked electrode model (PBE).[48]

RESULTS AND DISCUSSION

Film Evolution: Thickness and Internal Structure. Surface modifications using APTES and MPSA were carried over Au and Si substrates to anchor nucleation points suitable to trigger ZIF-8 heterogeneous nucleation. Although the exposed moieties (NH_2 for APTES and SO_3^- for MPSA) are different, ZIF-8 nucleation was demonstrated to be feasible in both cases and good quality films were already reported.[38,42,44,45] As mentioned before, ZIF-8 films were grown by the so-called one-pot LPE method. As shown in Figure 1a, the film growth was carried by repeating growth cycles, thus gradually increasing thickness. After the completion of each individual cycle, the film properties were analyzed. Hereafter, the films obtained after n growth cycles will be referred to as nx-ZIF-8, followed by @APTES or @MPSA, indicating the primer used.

Film growth was first analyzed via QCM-D, which has been already proved a powerful technique to this end.[34,49] As represented in Figure 1b, changes in the resonance frequency (f, Hz) of the quartz sensor can be related to the surface-bounded mass.[50] Additionally, the damping produced by viscoelastic materials can be interpreted in terms of the dissipation factor D, and the viscoelasticity of the films can thus be inferred; i.e., higher D values correspond to a viscoelastic behavior of the linked layer or "soft" films, while low D values can be associated with either rigid or elastic films coupled to resonator oscillation.[51] Au- and SiO_2-coated QCM sensors were modified with MPSA and APTES, respectively, and used as substrates for ex-situ ZIF-8 film growth (four samples prepared on each substrate were explored in order to ensure reproducibility). Considering primed sensor frequency as a reference, Δf values for dry films as a function of ZIF-8 growth cycles on both APTES- and MPSA-covered substrates were acquired, as shown in Figure 1c. Although both surface modification strategies followed triggered ZIF-8 film growth, there are clear differences. The Frequency change for the first growth cycle (*1x*-ZIF-8) is 4.7 times higher for MPSA than that for APTES. This can be ascribed to stronger interactions between SO_3^- moieties and Zn^{2+} ions, compared to the NH_2 decorated surface,[42,45] and to differences in the density of nucleation points introduced by the surface modification strategy employed. As expected, each modification strategy will decorate the substrates' surface with a different density of nucleation points, according to corresponding chemical characteristics. To highlight this difference, ellipsometric experiments were conducted for thickness determination and ultimately the optical mass density (Γ) of each nucleation layer through Lorentz−Lorenz approximation (see discussion in the Supporting Information (SI)). Notoriously, MPSA SAM renders $\Gamma_{MPSA} = 0.10\ \mu g\ cm^{-2}$, while APTES grafting renders an ~7 times higher mass density ($\Gamma_{APTES} = 0.66\ \mu g\ cm^{-2}$), yet MPSA decorated surfaces promote the ZIF-8 growth further. In other words, not only the density of nucleation points is relevant, but also the chemical interaction with ZIF-8 building units; MPSA generates a surface with a lower density of nucleation points than APTES but with stronger interactions (these points will be discussed again in the context of XRR experiments). The growth rate (in terms of frequency change, $\Delta f/\Delta n$, n = growth cycle) also shows clear differences; The MPSA primer layer promotes a linear $\Delta_{n=1-5}(\Delta f) = -745 \pm 9$ Hz/n increment; while for the APTES-functionalized surface Δf gradually increases from $\Delta_{n=1}(\Delta f) = -173$ Hz (for the first cycle) to $\Delta_{n=4-5}(\Delta f) = -681$ Hz (for the fifth cycle).

For uniform and rigid (elastic) films, Sauerbrey's equation can be employed to convert frequency changes into mass density changes Δm (see the SI), and ultimately a value of thickness can be inferred. A commonly accepted limit for Sauerbrey applicability is $\Delta D/(-\Delta f) < 0.2 \times 10^{-6}\ Hz^{-1}$, which ensures that D values do not depend on the resonance frequency of the sensor.[52] As shown in Figure 1d, both surface modifications employed yield rigid ZIF-8 films below such a limit. As a comparison, in Figure 1d, inset, the absolute D value is shown for each growth cycle and compared with the typical D values obtained for polyelectrolyte films built with a layer-by-layer method. This D value is typically accepted as the limit after which viscoelastic contributions cannot be neglected and Sauerbrey's formalism no longer applies.[52] It is safe to assume then that ZIF-8 films are rigid enough to be analyzed within this model (the progression of Δm as a function of growth cycles number can be found in the SI). Although film thickness will be analyzed below, together with ellipsometry results, it is worth emphasizing that, despite both primers used leading to thick and rigid ZIF-8 films, only MPSA yields linear and homogeneous growth progression, which suggests that their structure (and thus functional properties) might differ from each other.

The lateral structure, porosity, and thickness of films obtained were then explored with XRR and spectroscopic ellipsometry. As seen in Figure 2a, XRR profiles depict the position of critical angles q_c corresponding to substrates (q_c = 0.032 $Å^{-1}$ for Si and q_c = 0.077 $Å^{-1}$ for Au), together with

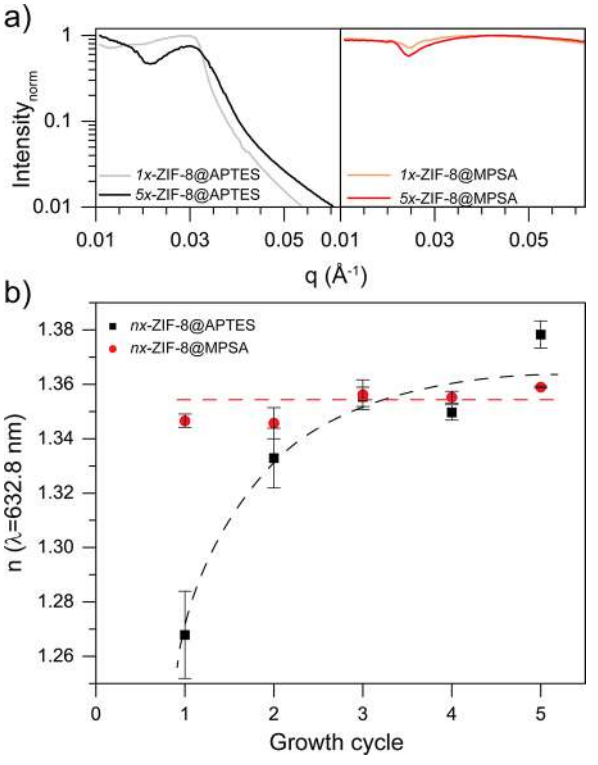

Figure 2. (a) X-ray reflectivity curves for *1x*- and *5x*-ZIF-8 films grown on APTES (left) and MPSA (right) surfaces. (b) Progression of ellipsometric refraction index of ZIF-8 films. Dashed lines are just eye guides. Error bars: Standard deviation of the mean.

https://doi.org/10.1021/acs.jpcc.1c10425
J. Phys. Chem. C 2022, 126, 6724−6735

additional features at lower q, ascribable to the ZIF-8 film.[37] As shown, no extra q_c is visible for the *1x*-ZIF-8@APTES sample, despite the presence of a film as described above. On the other hand, q_c for the *5x*-ZIF-8@APTES film is visible; this suggests that APTES promotes the growth of a rather inhomogeneous film that later becomes smoother with subsequent growth cycles. On the contrary, MPSA films are smooth and homogeneous enough to feature additional q_c corresponding to the ZIF-8 film even after only one growth cycle.

The XRR derived critical angle is proportional to the square of the mass density;[53] therefore, by comparing q_c values of the different films, their compactness can be assessed (see the SI for further details). Given the porous nature of ZIF-8, it is important to note that there are two main contributions to the total porosity: an intrinsic microporosity, provided by the ZIF-8 crystalline structure, and a so-called *constructional porosity* which depends on compactness achieved after synthesis.[54] This concept resembles the idea of "intergrain space", typically employed when dealing with bulk metallic materials or heterogeneous catalysts. However, constructional porosity results from the coalescence of multiple ZIF-8 growth fronts. Thus, it does not necessarily imply the presence of actual grains, but it generates additional (less hydrophobic) mesopores. Cracks or major defects present on the films do not fall in this category, given the differences in scale compared with micro- and mesopores.[55] Table 1 summarizes the critical

Table 1. Critical Angles q_c for ZIF-8 Films Grown Using Different Primers

nucleation layer	*n*x-	q_c (Å^{-1})	ref
APTES	1x-		this work
	5x-	0.0194	
MPSA	1x-	0.0240	this work
	5x-	0.0226	
PvIm brushes	5%	0.0199	37
	50%	0.0201	
	100%	0.0204	

angles obtained for *1x*- and *5x*-ZIF-8 films grown using APTES and MPSA as primer layers. As it can be seen, *1x*-ZIF-8@MPSA features the higher q_c value in the series, which means that it is the most compact film (higher density). The following value corresponds to *5x*-ZIF-8@MPSA; the effect of MPSA is expected to vanish as film growth proceeds, thus generating a less compact structure.[45] On the other hand, *5x*-ZIF-8@APTES films feature the lowest value of q_c, and given that the *1x*-ZIF-8@APTES film is not suitable for critical angle measurement, the compactness of the film is expected to be at least equal to or lower than that of *5x*-ZIF-8@APTES, which was later confirmed by spectroscopic ellipsometry (SE). In terms of nucleation points, MPSA surface modification seems to render a homogeneous distribution of nucleation points that promotes a homogeneous growth of ZIF-8 and, together with the stronger interaction of sulfonic moieties with zinc ions (compared with amino groups) yield thicker and compact films at each growth cycle.

For the sake of completeness, Table 1 shows previous results obtained using 3D primers (poly(1-vinylimidazole) brushes) as nucleation points, which allow tuning of the compactness of the film right between the values observed when using MPSA and APTES.[37] In this previous work, we have shown that the compactness of ZIF-8 films has a direct impact on the constructional porosity, with a lower hydrophobic character than intrinsic microporosity. Values of 5%, 50%, and 100% represent the grafting densities used for imidazolate-baring polymeric chains; the lower the value, the greater the space between those chains, which results in lower compactness of the resulting films or higher constructional porosity.

Quantification of microporosity and constructional porosity by comparing q_c values would require: (i) performing adsorption experiments with probe molecules accessing environments with different polarities (this presents additional complexity and does not necessarily probe the entire porosity of the film);[16] or (ii) a mass density value corresponding to a dense, nonporous ZIF-8 mass density that could be ascribed to the material's framework. Since ZIF-8 is naturally porous, access to the latter is not possible. The alternative thus is to use as a benchmark the most compact film of the series and to estimate the *additional* porosity of the remaining set (see the SI). Through this approach, it was possible to estimate that the *5x*-ZIF-8@MPSA film is 9.8% more porous than the *1x*-ZIF-8@MPSA film; the porosity of previously reported PvIm-based films ranges from 27% to 30% higher than the benchmark, and the *5x*-ZIF-8@APTES porosity is also 32.4% higher than the reference. Finally, *1x*-ZIF-8@APTES is expected to be at least as porous as *5x*-ZIF-8@APTES. The presence and role of the constructional porosity of the films will be discussed again in the context of CV electrochemical experiments.

The optical properties of the films can be related to their total porosity; thus, SE experiments were also conducted (see the SI for further details). SE experiments analysis require building an optical model describing the observed optical response of the film, which then is used to calculate its thickness and optical constants. Using a Cauchy layer to represent ZIF-8 film optical properties, given that neither Zn^{2+} nor mIm^- feature absorption bands in the spectral range explored, the refractive index at λ = 632.8 nm was obtained and compared with previous reports.[37,45] The progression of n (real part of the complex refractive index $\tilde{N} = n + ik$) as a function of growth cycles is shown in Figure 2b. As it can be seen, MPSA-based films display a rather constant value for n close to 1.35, which suggests that compactness does not change significantly as growth cycles proceed. On the other hand, the use of APTES as a primer does have an impact on the refractive index, which evolves toward a value close to the corresponding to MPSA (complete SE curves set can be found in the SI), in line with QCM and XRR findings above-discussed. MPSA provides a more effective primer layer, causing the films to grow homogeneously and thus resulting in uniform effective optical characteristics throughout the process. Each growth cycle can be thought of as a "gap filler" over the previous layer; in this way, the results obtained for APTES-primed surfaces in which films evolve from a less compact to a more compact structure can be rationalized. It is worth noting that, even for rather different film compactness, as determined via XRR, similar effective optical constants (see, e.g., 5x-films in Figure 2b) were obtained. The above discussion highlights the importance of a multitechnique approach for MOF films analysis, due to the existence of several interrelated properties which need to be determined for an unambiguous structure determination.

Film thickness evolution was determined from QCM experiments by using Sauerbrey's equation and a ZIF-8 mass density reference value δ = 0.95 g cm^{-3} (see the SI). Results are shown in Figure 3 together with thicknesses derived from

https://doi.org/10.1021/acs.jpcc.1c10425
J. Phys. Chem. C 2022, 126, 6724−6735

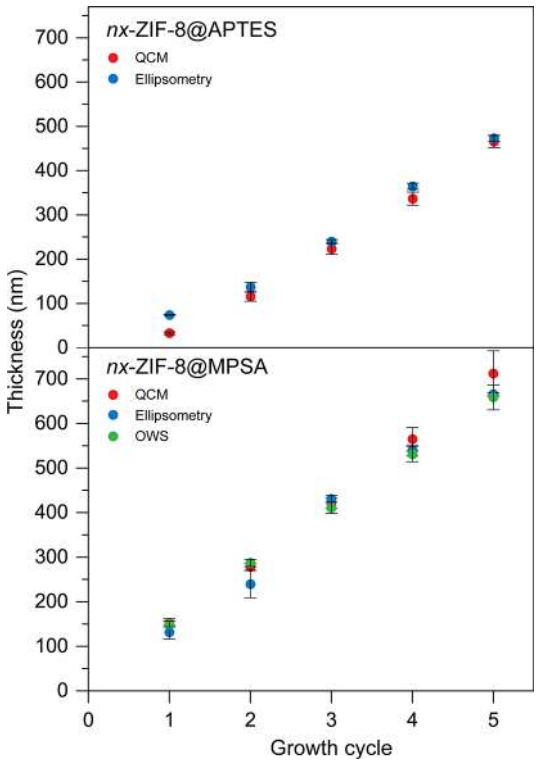

Figure 3. Thickness evolution of ZIF-8 films grown using APTES (top) and MPSA (bottom) primers as seen by QCM-D, spectroscopic ellipsometry, and previously reported values from optical waveguide spectroscopy.[45] Error bars: Standard deviation of the mean.

SE experiments and previously reported values from OWS.[45] As it can be seen, MPSA produces thicker films and linear growth. Films grew using APTES primer show systematically smaller initial growth rates of 80 and 90 nm/cycle (QCM- and SE-derived, respectively) in accordance with previous reports.[38] On the contrary, MPSA allows for a homogeneous thickness progression of 141, 134, and 138 nm/cycle (as obtained via QCM, SE, and OWS respectively).

Remarkably, although films with similar thicknesses could be in principle obtained using both primers by selecting an appropriate number of growth cycles (e.g., *2x*-ZIF-8@APTES and *1x*-ZIF-8@MPSA, or *5x*-ZIF-8@APTES and *3x*-ZIF-8@MPSA), this does not ensure that structures should be considered as comparable. As discussed above, compactness and optical properties evolve during consecutive growth cycles; thickness is not then a parameter that allows a direct comparison. It is worth noticing that three different techniques, based on different physical principles and approximations, provide comparable results, as clearly seen in Figure 3. This is not only a showcase of the reproducibility of the synthetic strategy followed but also reinforces the reliability of the data analysis applied.

Crystallinity, Roughness, and Surface Chemistry of Films. As discussed above, ZIF-8 is a crystalline material and the substrate used for film growth can not only affect the lateral structure of the film but also determine properties such as preferential crystalline orientation.[17,33,38,56] Thus, the crystallinity of the films obtained was analyzed by grazing-incidence (GI) XRD. GI-XRD might introduce artifacts on the obtained diffraction patterns, e.g., differences in integrated areas or Bragg positions shifts. To address these issues, the crystallinity of a powder (multioriented) ZIF-8 sample was analyzed in a Bragg−Brentano (B−B) configuration and compared with both the calculated XRD pattern and the same powder sample measured by GI-XRD upon casting it onto a gold substrate (Figure 4a). As shown, the material features the expected diffraction peaks and GI configuration does not affect significantly integrated areas, FWHM values, or peak positions (see the SI for details). Calculated lattice constants are in good agreement with previously reported values (a = 17.00 Å, 17.01 Å for B−B and GI measurements respectively).[20] Synthesized films were also analyzed by GI-XRD, and the results are shown in Figure 4b. As it can be seen, only *5x*- films were thick enough to generate a clear XRD pattern even at GI experiments; however, the (110) diffraction peak at ∼7.45° is visible for both *1x*- films, confirming their crystalline structure. Lattice constants obtained from GI measurements of the films are also in line with reported values (16.94 and 16.77 Å, for *5x*-ZIF-8@APTES and @MPSA, respectively). In addition, relative peak intensities and $FWHM_{(110)}$ were found to be similar for both systems, indicating no preferred crystalline orientation nor smaller/larger particle sizes (see the SI for details). To summarize, the films present the expected ZIF-8's ***sod*** crystalline structure with no significant differences upon the use of APTES or MPSA primers. As previously mentioned for thickness, crystallinity is not then a parameter that should be used for a direct comparison between films grown on different surfaces.

Although crystalline domains seem to be equivalent, AFM analysis of the films revealed a notoriously different surface morphology, as suggested by QCM, SE, and XRR results discussed above. Figure 4c shows AFM images of films taken at 5 μm side-scan areas for *1x*- and *5x*-, corresponding to the use of APTES and MPSA primers. It is evident from the images that APTES-modification lead to more inhomogeneous films, with big structures or agglomerations, while MPSA-modification provides a distribution of nucleation sites that evolve into smoother films. Height profiles and mean roughness (R_a) values (Figure 4d) are a clear indication of the above statement, although R_a value corresponds to *1x*-ZIF-8@MPSA is similar to what obtained when using APTES. Finally, *5x*-ZIF-8@MPSA has the lowest R_a value of the set and the smoothest height profile. Despite these differences, coverage of the substrate is complete in every case, regardless of the surface modification employed.

Effect of Surface Modification on the Molecular Transport through the Films. Molecular transport and permselectivity are two of the most appealing aspects of porous films and both can be addressed by resorting to electrochemical techniques.[43,46,47] In traditional mesoporous films obtained, e.g., by sol−gel chemistry, permselectivity relies on monodisperse mesoporosity featured by such templated materials.[57−62] For the hereby synthesized films, the analysis of molecular transport in aqueous environments possess a new degree of complexity, which is to unravel the above-discussed interplay between intrinsic microporosity and constructional (meso)porosity.[33,37,43−45,63] The difference in polarity between mainly hydrophobic microporosity (dictated by dangling methyl groups on ZIF-8 pore windows) and more hydrophilic constructional porosity arises from partially coordinated 2-methylimidazole and zinc terminal sites (hydroxylated after exposure to aqueous environments)[64] exposed on ZIF-8, as schematized in Figure 5a.[63,65,66]

To perform these analyses, films need to be deposited onto conductive substrates, that allow the CV measurements. To

https://doi.org/10.1021/acs.jpcc.1c10425
J. Phys. Chem. C 2022, 126, 6724−6735

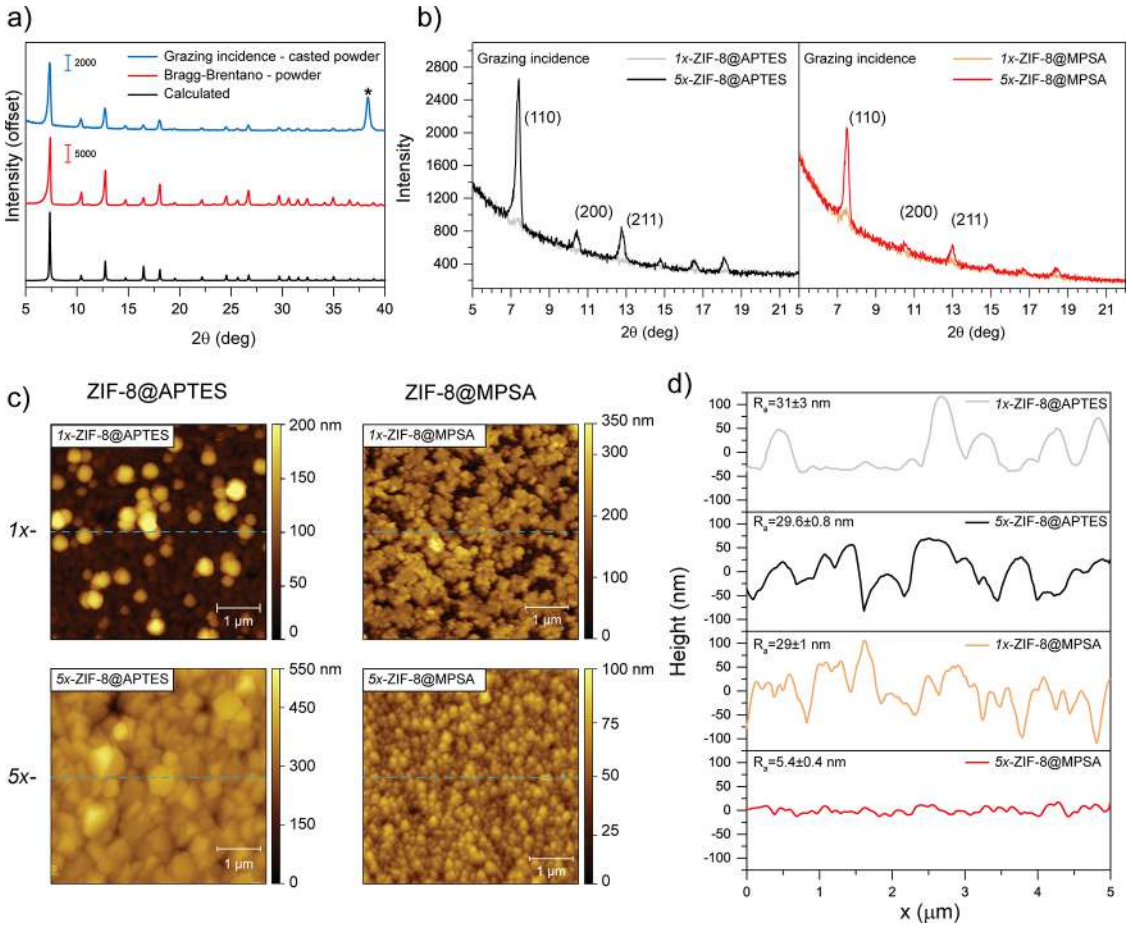

Figure 4. (a) Calculated XRD diffraction pattern for ZIF-8 together with ZIF-8 powder sample (Bragg−Brentano configuration) and the same powder measured by grazing incidence upon casting on a gold substrate. (b) Grazing-incidence XRD diffraction pattern for *1x*- and *5x*-ZIF-8 films grown on APTES (left) and MPSA (right). (c) 5 μm side AFM scans for *1x*- and *5x*-ZIF-8 films grown on APTES (left) and MPSA (right). (d) Height profiles for images in (c) at dashed blue lines together with R_a values for each surface.

that end, samples in which APTES was used as primer were prepared onto ITO modified glass (see Methods for details). By ellipsometric experiments, APTES grafting was found to be equivalent on ITO and Si substrates, and thus, the density of nucleation points between both substrates is equivalent. Since the substrate own chemistry may have an impact on the characteristics of the film, *1x*- and *5x*-ZIF-8@APTES/ITO films were also characterized by XRR to determine their critical angles. The obtained results (see the SI for details) indicate that the films prepared on APTES-grafted ITO present an equivalent critical angle to the ones obtained onto Si and, consequently, equivalent electronic density (i.e., compactness). Thus, ITO supported films can be considered equivalent to Si supported samples and can be safely used for permeability experiments.

It is known that porous films might undergo dissolution and degradation by in-operando conditions used in aqueous environments.[67,68] Having this in mind, and although *5x*-ZIF-8@MPSA films were already proved to be stable under moderate ionic strength aqueous environments,[45] the first issue we addressed here was whether permeation through films depended on contact time with aqueous environments or not. Considering the already reported charge-exclusion effect for ZIF-8 films for the diffusion of negatively charged redox probes,[44] the above issue can be tackled. A *5x*-ZIF-8@MPSA film grown on a gold QCM electrode was exposed to hexacyanoferrate redox probe solution for 24 h while applying voltage in a typical CV experiment. As shown in Figure 5b (top), the current density at E = 0.250 V due to $Fe(CN)_6^{4-}$ redox probe is almost constant and almost 35 times lower than the current density expected for the bare gold electrode. Furthermore, changes in resonance frequency in dry conditions revealed that no significant mass loss took place after 24 h CV experiment, as shown in Figure 5b (bottom). The QCM device employed before for dissipation studies did not allow in situ electrochemical measurements, and thus, a different setup was used. Here, viscoelastic behavior was analyzed in terms of the motion resistance ΔR (Figure 5b bottom right axis) of the film in dry conditions. ΔR is directly related to viscoelastic behavior,[69−71] and since we demonstrate that ZIF-8 films behave as rigid films by dissipation studies, the 7% decrease in ΔR indicates no significant changes in the elasticity of the film (see the SI for a more detailed discussion of motional resistance). To summarize, these results demonstrate that ZIF-8 films are stable toward electrochemical cycling conditions herein employed and that permeability studies will not depend on exposure periods to an aqueous environment nor have any effect on the structural properties of the films.

We then performed experiments oriented to analyze molecular transport using noncharged (ferrocenemethanol, FcMeOH hereinafter) and negatively charged (potassium ferrocyanide (II) and potassium ferricyanide (III) solution,

https://doi.org/10.1021/acs.jpcc.1c10425
J. Phys. Chem. C 2022, 126, 6724−6735

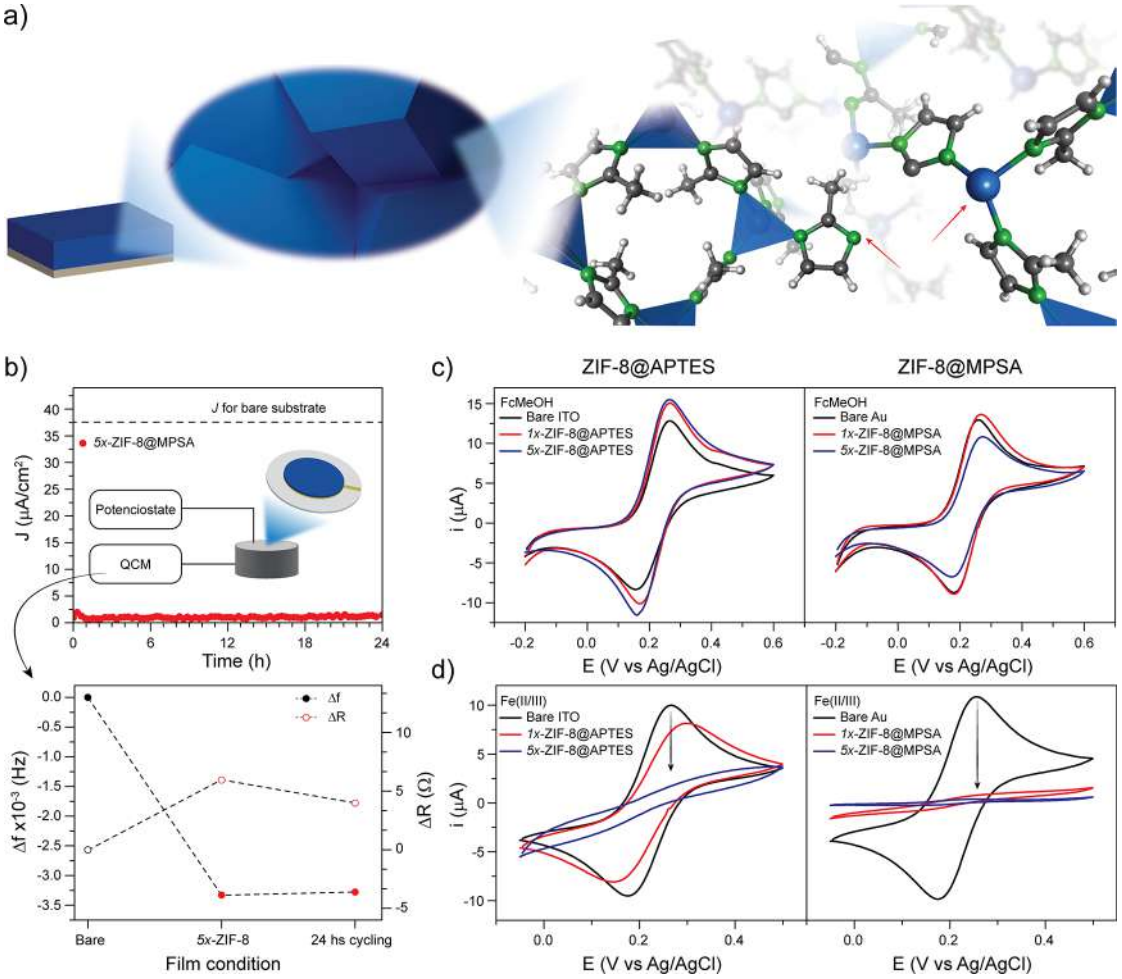

Figure 5. (a) Schematic representation of internal structure and coordinately unsaturated groups across ZIF-8 films. (b, top) Evolution of current density at E = 0.250 V vs Ag/AgCl with cycling time for *5x*-ZIF-8@MPSA film using 1 mM Fe(II/III) solution for CV experiments on QCM electrode. (b, bottom) Changes in frequency (left) and motion resistance (right) for the film (dry conditions) before and after 24 h cycling in Fe(II/III) solution. Cyclic voltammetry experiments at 5 mV/s on ZIF-8 films using 2 mM solutions of (c) ferrocenemethanol (FcMeOH) and (d) potassium ferro/ferricyanide (Fe(II/III)) redox probes.

Fe(II/III) hereinafter) redox probes. CV experiments were conducted using *1x*- and *5x*- ZIF-8 films grown on APTES-grafted ITO electrodes and MPSA-modified gold electrodes. There are major differences between both probes, as results summarized in Figure 5c,d show. None of the explored films seem to significantly affect the diffusion of FcMeOH toward the electrode surface (Figure 5c). On the contrary, all the films explored block up to some point Fe(II/III) diffusion (Figure 5d). Given the similar kinetic diameters of probes used,[72] this difference can only be rationalized by resorting to charge-exclusion effects.[44]

Typically, quantification of molecular transport through porous films is addressed by analyzing cyclic voltammetry experiments in terms of the Randles−Ševčik (RS) formalism, as described in the SI; however, *5x*-ZIF-8@MPSA films cannot be modeled using RS. There is a strong deviation from expected linearity in the I vs $\nu^{1/2}$ plots, as well as changes in the CV shape. This means that the diffusion regime changes with the scan rate used and that the film-modified substrates behave as partially blocked electrodes (PBE).[48] PBE refers to a situation in which the electrode geometrical area is not equivalent to the active area. Briefly, conductive substrates modified by ZIF-8 films can be seen as an array of spatially distributed microelectrodes with different percentages of surface blockage due to the presence of the porous film.[73] Constructional porosity modifies center-to-center distance and the size of such microelectrodes, ultimately affecting the dominating diffusion regime operating, as schematized in Figure 6a. Those changes can be qualitatively accounted for by normalizing voltammograms and analyzing changes in their shape, in addition to considering the corresponding absolute current values. A full description of this approach can be found in the SI.

Applying PBE analysis to FcMeOH CV experiments, it was observed that *1x*-ZIF-8@APTES film produces a low coverage of electrode surface (Figure 6b, top); voltammograms do not change in shape compared with the bare electrode at any of the explored scan rates. This is an indication of a planar diffusion regime over a low coverage PBE, i.e., large microelectrodes and/or short center-to-center distances among them, which leads to complete overlap of diffusion layers of individual microelectrodes. However, the voltammograms obtained with *5x*-ZIF-8@APTES do change their shape for increasingly higher scan rates and, at the same time, the I vs $\nu^{1/2}$ plot deviates from linearity (see the SI). Such behavior is expected when the individual microelectrode size is smaller and/or

https://doi.org/10.1021/acs.jpcc.1c10425
J. Phys. Chem. C 2022, 126, 6724−6735

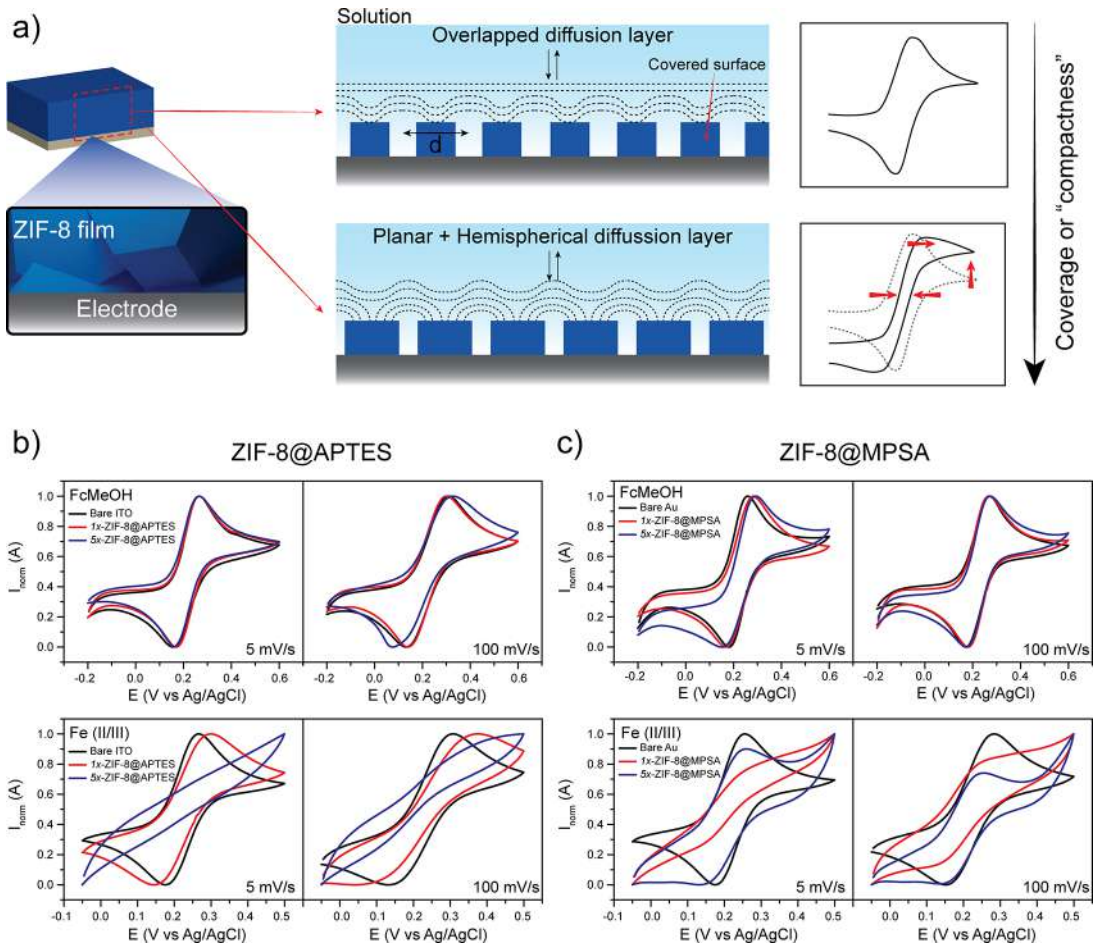

Figure 6. (a) Schematic representation of ZIF-8 films as seen as microelectrode arrays, together with expected shape changes in voltagramms with coverage or "compactness" of the films (d: center-to-center distance of individual microelectrodes). Normalized voltammograms using FcMeOH and Fe(II/III) redox probes on (b) ZIF-8@APTES films and (c) ZIF-8@MPSA films.

center-to-center distance becomes larger; i.e., the compactness of the film increases. In other words, coverage of the electrode surface is greater. As compactness increases, diffusion layers of neighboring microelectrodes start to separate, creating a mixed planar + hemispherical diffusion regime. The same behavior was found for ZIF-8@MPSA films; however, the *1x*-ZIF-8@MPSA film already had differences with the bare substrate (Figure 6c, top), indicating higher compactness of *1x*-ZIF-8@MPSA compared with APTES-based films. For the sake of comparison, and considering that FcMeOH experiments on APTES-based films and *1x*-ZIF-8@MPSA can also be interpreted in terms of the RS formalism, effective diffusion coefficients (D_{eff}) were calculated (see the SI). The results are consistent with the case in which an overlapped planar diffusion layer with the same geometrical area as the bare electrode is present. Since some variability in the electrochemical response of substrate is expected, and differences among D_{eff} values may not be significant.[48]

As mentioned above, all ZIF-8 films present charge-exclusion behavior toward negatively charged probes, being far more pronounced the effect on MPSA-primed films, and none of them can be interpreted by RS formalism. However, charge-exclusion behavior can be interpreted using the PBE analysis as an "effective" coverage larger than the real coverage; in other words, electrostatic repulsion between ZIF-8 pore walls corresponding to CP and the redox probe will block the smaller channels for probe diffusion, thus mimicking the result expected for a more compact film. For *1x*-ZIF-8@APTES films, changes in the voltammograms shape are seen when using low (5 mV/s) and high (100 mV/s) scan rates, as shown in Figure 6b, bottom. Here, mixed planar + hemispherical diffusion regimes can be inferred. For the other films, i.e., *5x*-ZIF-8@APTES and both *1x*- and *5x*-ZIF-8@MPSA (Figure 6c, bottom), the blockage is stronger and PBE analysis cannot be applied. The film structure affects probe diffusion in a way much more like a homogeneous and continuous membrane hindering transport toward the electrode surface, with this being the limiting process that dominates mass transfer.[74,75]

CONCLUSIONS

In this work, we have shown how surface chemistry determines the growth rate, compactness and functional properties of ZIF-8 films synthesized by the straightforward one-pot liquid phase epitaxial method. Different characterization techniques were employed to address each different feature of the films, which are summarized in Table 2.

We have demonstrated the effect of the nucleation layer on the structural and functional characteristics of the ZIF-8- films. Although both surface modifications explored yield continuous ZIF-8 films, the MPSA self-assembled monolayer, with ~7 lower mass density than APTES but stronger interaction with Zn^{2+}, enables a constant and uniform growth rate (average 132

https://doi.org/10.1021/acs.jpcc.1c10425
J. Phys. Chem. C 2022, 126, 6724−6735

Table 2. Summary of Main Characterization Features of the Explored Films[a]

	@APTES		@MPSA	
main features	1x-ZIF-8	5x-ZIF-8	1x-ZIF-8	5x-ZIF-8
$\Delta F/n$, Hz (QCM)	−173	−2463	−808	−3769
$\Delta m/n$, $\mu g \cdot cm^{-2}$ (QCM)	3.1	44.2	14.5	67.7
thickness, nm (QCM)	33	465	153	712
thickness, nm (ellipsometry)	74	473	132	665
refraction index λ = 632.8 nm (ellipsometry)	1.2679	1.3783	1.3466	1.3590
q_c, $Å^{-1}$ (XRR)	-	0.0194	0.0240	0.0226
$FWHM_{(110)}$ (GI-XRD)	-	0.249	-	0.253
R_a, nm (AFM)	31	30	29	5

[a] q_c: Critical angle. FWHM: Full Width at Half Maximum. R_a: Surface roughness.

± 2 nm/cycle) and higher thicknesses after every growth cycle compared to APTES (on average, the growth rate varies from 61 ± 6 to 119 ± 14 nm/cycle). This progression in the growth rate indicates that the nucleation layer has an effect on the first growth cycle and then the previously grown film serves as a nucleation point for the subsequent cycles. Despite these differences in growth rates, by choosing an appropriate number of growth cycles, films with similar thicknesses can be achieved for both primed substrates. Interestingly, even when no differences were detected in terms of crystallinity of those films, the film compactness is highly dependent on the primer and is not directly related to the film thickness, rendering the so-called constructional porosity. The constructional porosity present in the synthesized films was found to be a determinant for molecular transport. Our analysis of permeation in terms of the PBE model reveals that using APTES as the primer causes an increased permeability compared to MPSA-primed films. In other words, the MPSA nucleation layer leads to a more compact and uniform film.

Our results also stress the relevance of a multitechnique approach toward film characterization if functional properties arising from different synthetic procedures are to be properly addressed. Neither thickness nor crystallinity alone (two of the most commonly employed indicators of a film condition) revealed the structural differences present. We have shown that these differences cannot be disregarded, since they dominate the functional properties of the films and that functional properties are strongly influenced by the nucleation layer employed. Thus, by careful selection of primers compatible with different modes of MOF growth, film structure (and thus transport properties, crucial for any application based on porosity) can be successfully modulated.

METHODS

Materials. Anhydrous methanol was obtained from commercial methanol as described in the SI. Sulfuric acid, zinc nitrate hexahydrate $Zn(NO_3)_2 \cdot 6H_2O$, 2-methylimidazole (HmIm), (3-aminopropyl)triethoxysilane (APTES), and 3-mercapto-1-propanesulfonic acid (MPSA) were purchased from Sigma-Aldrich and used without further purification. Hydrogen peroxide, potassium chloride, potassium hexacyanoferrate (II) and (III), and ferrocenemethanol were purchased from Anedra and used without further purification. Solutions for electrochemical experiments were prepared with ultrapure Milli-Q water (18.24 MΩ cm^{-1}).

Characterization Techniques. Quarz crystal microbalance (QCM-D) and spectroscopic ellipsometry (SE) were employed to characterize film growth; X-ray reflectometry (XRR) and grazing-incidence X-ray diffraction (GI-XRD) were used for lateral structure, porosity, and crystallinity characterization of the films. X-ray photoelectron spectroscopy (XPS) and atomic force microscopy (AFM) were employed to characterize surface chemistry and topology. Cyclic voltammetry (CV) experiments were conducted in a three-electrode cell, and the results were analyzed via the partially blocked electrode model (PBE). A complete description of the equipment and methodology can be found in the SI.

ZIF-8 Film Synthesis. *Substrate Preparation.* Silicon slides of ∼1 × 2.5 cm^2 where cut from 76.2 mm diameter single-side polished wafers. Substrates were then cleaned with acid piranha solution (***Caution**: Piranha solution is a very strong oxidant and is dangerous to handle without appropriate personal protection elements*), washed thoroughly with Milli-Q water, and dried at 120 °C. Silanization was carried out by immersing substrates in 0.2 mM APTES toluene solution at 80 °C for 4 h.[76] After silanization, substrates were washed with toluene and placed in an oven at 120 °C for 2 h for thermal annealing. Conductive ITO substrates were modified using the same procedure, but piranha treatment was replaced by a three-step immersion in an ultrasonic bath with soapy water, Milli-Q water, and ethanol. Gold substrates (∼1 × 2.5 cm^2) were immersed briefly in diluted acid piranha solution, washed with Milli-Q water, and dried in a N_2 stream. MPSA modification was carried by immersing the substrates in a 20 mM MPSA solution in 16 mM H_2SO_4 aqueous solution for 30 min. Substrates were then washed with 16 mM H_2SO_4 aqueous solution and then Milli-Q water and dried under N_2 stream.[45,77]

ZIF-8 Film Growth. ZIF-8 films were prepared following procedures previously reported.[44,45] Briefly, modified substrates were placed in a glass vial at 25 °C as shown in Figure 1a, with the functionalized surface facing down. Then 25 mM $Zn(NO_3)_2 \cdot 6H_2O$ methanolic solution was added, covering the entire substrate. Then, an equal volume of 50 mM HmIm methanolic solution was promptly added, ensuring proper mixing. The final molar ratio was 1(Zn):2(HmIm):1978(methanol). After 30 min, the substrates were washed with methanol and dried under a N_2 stream. These steps constitute one growth cycle (n). By repeating the described cycle, the final film thickness can be increased.

ASSOCIATED CONTENT

Supporting Information

The Supporting Information is available free of charge at https://pubs.acs.org/doi/10.1021/acs.jpcc.1c10425.

Experimental details; further information on characterization techniques; QCM mass density calculation, Sauerbrey's and motion resistance experiments details; porosity estimation by XRR; XRD information; XPS surface characterization; electrochemical experiments and partially blocked electrode theory (PDF)

AUTHOR INFORMATION

Corresponding Authors

Juan A. Allegretto − *Instituto de Investigaciones Fisicoquímicas Teóricas y Aplicadas (INIFTA), Departamento de Química, Facultad de Ciencias Exactas,*

https://doi.org/10.1021/acs.jpcc.1c10425
J. Phys. Chem. C 2022, 126, 6724−6735

Universidad Nacional de La Plata, CONICET, La Plata B1904DPI, Argentina; Universidad Nacional de San Martin (UNSAM), San Martín B1650, Argentina; orcid.org/0000-0002-7371-2610; Email: allegretto@inifta.unlp.edu.ar

Matias Rafti − *Instituto de Investigaciones Fisicoquímicas Teóricas y Aplicadas (INIFTA), Departamento de Química, Facultad de Ciencias Exactas, Universidad Nacional de La Plata, CONICET, La Plata B1904DPI, Argentina;* orcid.org/0000-0003-3393-358X; Email: mrafti@inifta.unlp.edu.ar

Authors

Melina Arcidiácono − *Instituto de Investigaciones Fisicoquímicas Teóricas y Aplicadas (INIFTA), Departamento de Química, Facultad de Ciencias Exactas, Universidad Nacional de La Plata, CONICET, La Plata B1904DPI, Argentina;* orcid.org/0000-0002-3993-1000

Paula Y. Steinberg − *Gerencia Química, Centro Atómico Constituyentes, Comisión Nacional de Energía Atómica, San Martín B1650, Argentina;* orcid.org/0000-0001-5857-7046

Paula C. Angelomé − *Instituto de Nanociencia y Nanotecnología, CONICET-CNEA, San Martín B1650, Argentina; Gerencia Química, Centro Atómico Constituyentes, Comisión Nacional de Energía Atómica, San Martín B1650, Argentina;* orcid.org/0000-0002-4402-5045

Omar Azzaroni − *Instituto de Investigaciones Fisicoquímicas Teóricas y Aplicadas (INIFTA), Departamento de Química, Facultad de Ciencias Exactas, Universidad Nacional de La Plata, CONICET, La Plata B1904DPI, Argentina;* orcid.org/0000-0002-5098-0612

Complete contact information is available at: https://pubs.acs.org/10.1021/acs.jpcc.1c10425

Notes

The authors declare no competing financial interest.

■ ACKNOWLEDGMENTS

J.A.A. and M.A. want to acknowledge CONICET for a doctoral scholarship. P.C.A., O.A., and M.R. are CONICET staff members. P.Y.S. acknowledges CONICET for a postdoctoral scholarship. Financial support from Universidad Nacional de La Plata (Project PPID/X026) and Agencia Nacional de Promoción Científica y Tecnológica (ANPCyT, PICT-2018-00780 & PICT-2019-01615) is gratefully acknowledged.

■ REFERENCES

(1) Hoskins, B. F.; Robson, R. Infinite polymeric frameworks consisting of three dimensionally linked rod-like segments. *J. Am. Chem. Soc.* **1989**, *111*, 5962−5964.

(2) Yaghi, O. M.; Li, H. Hydrothermal Synthesis of a Metal-Organic Framework Containing Large Rectangular Channels. *J. Am. Chem. Soc.* **1995**, *117*, 10401−10402.

(3) Moghadam, P. Z.; Li, A.; Wiggin, S. B.; Tao, A.; Maloney, A. G.; Wood, P. A.; Ward, S. C.; Fairen-Jimenez, D. Development of a Cambridge Structural Database Subset: A Collection of Metal-Organic Frameworks for Past, Present, and Future. *Chem. Mater.* **2017**, *29*, 2618−2625.

(4) Maurin, G.; Serre, C.; Cooper, A.; Férey, G. The new age of MOFs and of their porous-related solids. *Chem. Soc. Rev.* **2017**, *46*, 3104−3107.

(5) Furukawa, S.; Reboul, J.; Diring, S.; Sumida, K.; Kitagawa, S. Structuring of metal−organic frameworks at the mesoscopic/macroscopic scale. *Chem. Soc. Rev.* **2014**, *43*, 5700−5734.

(6) Kreno, L. E.; Leong, K.; Farha, O. K.; Allendorf, M.; Van Duyne, R. P.; Hupp, J. T. Metal-organic framework materials as chemical sensors. *Chem. Rev.* **2012**, *112*, 1105−1125.

(7) Falcaro, P.; Ricco, R.; Doherty, C. M.; Liang, K.; Hill, A. J.; Styles, M. J. MOF positioning technology and device fabrication. *Chem. Soc. Rev.* **2014**, *43*, 5513−5560.

(8) Stassen, I.; Burtch, N.; Talin, A.; Falcaro, P.; Allendorf, M.; Ameloot, R. An updated roadmap for the integration of metal-organic frameworks with electronic devices and chemical sensors. *Chem. Soc. Rev.* **2017**, *46*, 3185−3241.

(9) Li, W. J.; Tu, M.; Cao, R.; Fischer, R. A. Metal-organic framework thin films: Electrochemical fabrication techniques and corresponding applications & perspectives. *Journal of Materials Chemistry A* **2016**, *4*, 12356−12369.

(10) Zhuang, J. L.; Terfort, A.; Wöll, C. Formation of oriented and patterned films of metal-organic frameworks by liquid phase epitaxy: A review. *Coord. Chem. Rev.* **2016**, *307*, 391−424.

(11) Liu, J.; Wöll, C. Surface-supported metal-organic framework thin films: Fabrication methods, applications, and challenges. *Chem. Soc. Rev.* **2017**, *46*, 5730−5770.

(12) Wang, Z.; Wöll, C. Fabrication of Metal−Organic Framework Thin Films Using Programmed Layer-by-Layer Assembly Techniques. *Adv. Mater. Technol.* **2019**, *4*, 1800413.

(13) Shekhah, O.; Wang, H.; Kowarik, S.; Schreiber, F.; Paulus, M.; Tolan, M.; Sternemann, C.; Evers, F.; Zacher, D.; Fischer, R. A.; et al. Step-by-step route for the synthesis of metal-organic frameworks. *J. Am. Chem. Soc.* **2007**, *129*, 15118−15119.

(14) Shekhah, O.; Wang, H.; Strunskus, T.; Cyganik, P.; Zacher, D.; Fischer, R.; Wöll, C. Layer-by-layer growth of oriented metal organic polymers on a functionalized organic surface. *Langmuir* **2007**, *23*, 7440−7442.

(15) Liu, B.; Fischer, R. A. Liquid-phase epitaxy of metal organic framework thin films. *Science China Chemistry* **2011**, *54*, 1851−1866.

(16) Heinke, L.; Gu, Z.; Wöll, C. The surface barrier phenomenon at the loading of metal-organic frameworks. *Nat. Commun.* **2014**, *5*, 4562.

(17) Shekhah, O.; Eddaoudi, M. The liquid phase epitaxy method for the construction of oriented ZIF-8 thin films with controlled growth on functionalized surfaces. *Chem. Commun.* **2013**, *49*, 10079−10081.

(18) Liu, J.; Paradinas, M.; Heinke, L.; Buck, M.; Ocal, C.; Mugnaini, V.; Wöll, C. Film Quality and Electronic Properties of a Surface-Anchored Metal-Organic Framework Revealed by using a Multi-technique Approach. *ChemElectroChem.* **2016**, *3*, 713−718.

(19) Chernikova, V.; Shekhah, O.; Eddaoudi, M. Advanced Fabrication Method for the Preparation of MOF Thin Films: Liquid-Phase Epitaxy Approach Meets Spin Coating Method. *ACS Appl. Mater. Interfaces* **2016**, *8*, 20459−20464.

(20) Park, K. S.; Ni, Z.; Cote, A. P.; Choi, J. Y.; Huang, R.; Uribe-Romo, F. J.; Chae, H. K.; O'Keeffe, M.; Yaghi, O. M. Exceptional chemical and thermal stability of zeolitic imidazolate frameworks. *Proc. Natl. Acad. Sci. U. S. A.* **2006**, *103*, 10186−10191.

(21) Chmelik, C. Characteristic features of molecular transport in MOF ZIF-8 as revealed by IR microimaging. *Microporous Mesoporous Mater.* **2015**, *216*, 138−145.

(22) James, J. B.; Lin, Y. S. Kinetics of ZIF-8 Thermal Decomposition in Inert, Oxidizing, and Reducing Environments. *J. Phys. Chem. C* **2016**, *120*, 14015−14026.

(23) Zhang, K.; Lively, R. P.; Zhang, C.; Chance, R. R.; Koros, W. J.; Sholl, D. S.; Nair, S. Exploring the framework hydrophobicity and flexibility of zif-8: From biofuel recovery to hydrocarbon separations. *J. Phys. Chem. Lett.* **2013**, *4*, 3618−3622.

(24) Liu, X.; Jin, H.; Li, Y.; Bux, H.; Hu, Z.; Ban, Y.; Yang, W. Metal-organic framework ZIF-8 nanocomposite membrane for efficient recovery of furfural via pervaporation and vapor permeation. *J. Membr. Sci.* **2013**, *428*, 498−506.

(25) Kim, K. J.; Lu, P.; Culp, J. T.; Ohodnicki, P. R. Metal-Organic Framework Thin Film Coated Optical Fiber Sensors: A Novel Waveguide-Based Chemical Sensing Platform. *ACS Sensors* **2018**, *3*, 386−394.
(26) Chocarro-Ruiz, B.; Pérez-Carvajal, J.; Avci, C.; Calvo-Lozano, O.; Alonso, M. I.; Maspoch, D.; Lechuga, L. M. A CO2 optical sensor based on self-assembled metal-organic framework nanoparticles. *Journal of Materials Chemistry A* **2018**, *6*, 13171−13177.
(27) Chizallet, C.; Lazare, S.; Bazer-Bachi, D.; Bonnier, F.; Lecocq, V.; Soyer, E.; Quoineaud, A.-A.; Bats, N. Catalysis of Transesterification by a Nonfunctionalized Metal-Organic Framework: Acido-Basicity at the External Surface of ZIF-8 Probed by FTIR and ab Initio Calculations. *J. Am. Chem. Soc.* **2010**, *132*, 12365−12377.
(28) Tran, U. P.; Le, K. K.; Phan, N. T. Expanding applications of metal-organic frameworks: Zeolite imidazolate framework zif-8 as an efficient heterogeneous catalyst for the knoevenagel reaction. *ACS Catal.* **2011**, *1*, 120−127.
(29) Yadav, D. K.; Gupta, R.; Ganesan, V.; Sonkar, P. K.; Yadav, M. Gold Nanoparticles Incorporated in a Zinc-Based Metal-Organic Framework as Multifunctional Catalyst for the Oxygen Reduction and Hydrogen Evolution Reactions. *ChemElectroChem.* **2018**, *5*, 2612−2619.
(30) Rafti, M.; Marmisollé, W. A.; Azzaroni, O. Metal-Organic Frameworks Help Conducting Polymers Optimize the Efficiency of the Oxygen Reduction Reaction in Neutral Solutions. *Adv. Mater. Interfaces* **2016**, *3*, 1600047.
(31) Fenoy, G. E.; Scotto, J.; Azcárate, J.; Rafti, M.; Marmisollé, W. A.; Azzaroni, O. Powering Up the Oxygen Reduction Reaction through the Integration of O2-Adsorbing Metal-Organic Frameworks on Nanocomposite Electrodes. *ACS Appl. Energy Mater.* **2018**, *1*, 5428−5436.
(32) Lu, G.; Hupp, J. T. Metal-organic frameworks as sensors: A ZIF-8 based fabry-pérot device as a selective sensor for chemical vapors and gases. *J. Am. Chem. Soc.* **2010**, *132*, 7832−7833.
(33) Eslava, S.; Zhang, L.; Esconjauregui, S.; Yang, J.; Vanstreels, K.; Baklanov, M. R.; Saiz, E. Metal-organic framework ZIF-8 films as low-κ dielectrics in microelectronics. *Chem. Mater.* **2013**, *25*, 27−33.
(34) Shen, D.; Ma, X.; Cai, T.; Zhu, X.; Xin, X.; Kang, Q. Investigation on kinetic processes of zeolitic imidazolate framework-8 film growth and adsorption of chlorohydro-carbons using a quartz crystal microbalance. *Analytical Methods* **2015**, *7*, 9619−9628.
(35) Rafti, M.; Allegretto, J. A.; Segovia, G. M.; Tuninetti, J. S.; Giussi, J. M.; Bindini, E.; Azzaroni, O. Metal-organic frameworks meet polymer brushes: Enhanced crystalline film growth induced by macromolecular primers. *Materials Chemistry Frontiers* **2017**, *1*, 2256−2260.
(36) Hou, L.; Zhou, M.; Dong, X.; Wang, L.; Xie, Z.; Dong, D.; Zhang, N. Controlled Growth of Metal-Organic Frameworks on Polymer Brushes. *Chem.—Eur. J.* **2017**, *23*, 13337−13341.
(37) Allegretto, J. A.; Iborra, A.; Giussi, J. M.; von Bilderling, C.; Ceolín, M.; Moya, S.; Azzaroni, O.; Rafti, M. Growth of ZIF-8 MOF Films with Tunable Porosity by using Poly (1-vinylimidazole) Brushes as 3D Primers. *Chem.—Eur. J.* **2020**, *26*, 12388−12396.
(38) Hou, C.; Xu, Q.; Peng, J.; Ji, Z.; Hu, X. 110)-Oriented ZIF-8 thin films on ITO with controllable thickness. *ChemPhysChem* **2013**, *14*, 140−144.
(39) Kida, K.; Fujita, K.; Shimada, T.; Tanaka, S.; Miyake, Y. Layer-by-layer aqueous rapid synthesis of ZIF-8 films on a reactive surface. *Dalton Transactions* **2013**, *42*, 11128−11135.
(40) Kong, L.; Zhang, G.; Liu, H.; Zhang, X. APTES-assisted synthesis of ZIF-8 films on the inner surface of capillary quartz tubes via flow system. *Mater. Lett.* **2015**, *141*, 344−346.
(41) Li, S.; Shi, W.; Lu, G.; Li, S.; Loo, S. C. J.; Huo, F. Unconventional nucleation and oriented growth of ZIF-8 crystals on non-polar surface. *Adv. Mater.* **2012**, *24*, 5954−5958.
(42) Tuninetti, J. S.; Rafti, M.; Azzaroni, O. Early stages of ZIF-8 film growth: the enhancement effect of primers exposing sulfonate groups as surface-confined nucleation agents. *RSC Adv.* **2015**, *5*, 73958−73962.
(43) Tuninetti, J. S.; Rafti, M.; Andrieu-Brunsen, A.; Azzaroni, O. Molecular transport properties of ZIF-8 thin films in aqueous environments: The critical role of intergrain mesoporosity as diffusional pathway. *Microporous Mesoporous Mater.* **2016**, *220*, 253−257.
(44) Allegretto, J. A.; Tuninetti, J. S.; Lorenzo, A.; Ceolín, M.; Azzaroni, O.; Rafti, M. Polyelectrolyte Capping As Straightforward Approach toward Manipulation of Diffusive Transport in MOF Films. *Langmuir* **2018**, *34*, 425−431.
(45) Allegretto, J. A.; Dostalek, J.; Rafti, M.; Menges, B.; Azzaroni, O.; Knoll, W. Shedding Light on the Dark Corners of Metal-Organic Framework Thin Films: Growth and Structural Stability of ZIF-8 Layers Probed by Optical Waveguide Spectroscopy. *J. Phys. Chem. A* **2019**, *123*, 1100−1109.
(46) Calvo, A.; Yameen, B.; Williams, F. J.; Azzaroni, O.; Soler-Illia, G. J. A. A. Facile molecular design of hybrid functional assemblies with controllable transport properties: mesoporous films meet polyelectrolyte brushes. *Chem. Commun.* **2009**, 2553.
(47) Brunsen, A.; Calvo, A.; Williams, F. J.; Soler-Illia, G. J. A. A.; Azzaroni, O. Manipulation of Molecular Transport into Mesoporous Silica Thin Films by the Infiltration of Polyelectrolytes. *Langmuir* **2011**, *27*, 4328−4333.
(48) Steinberg, P. Y.; Zanotto, F. M.; Soler-Illia, G. J.; Dassie, S. A.; Angelomé, P. C. Molecular Transport through TiO 2 Mesoporous Thin Films: Correlation with the Partially Blocked Electrode Model. *J. Phys. Chem. C* **2021**, *125*, 23521−23532.
(49) Stavila, V.; Volponi, J.; Katzenmeyer, A. M.; Dixon, M. C.; Allendorf, M. D. Kinetics and mechanism of metal−organic framework thin film growth: systematic investigation of HKUST-1 deposition on QCM electrodes. *Chemical Science* **2012**, *3*, 1531.
(50) Marx, K. A. Quartz Crystal Microbalance: A Useful Tool for Studying Thin Polymer Films and Complex Biomolecular Systems at the Solution-Surface Interface. *Biomacromolecules* **2003**, *4*, 1099−1120.
(51) Johannsmann, D.; Reviakine, I.; Richter, R. P. Dissipation in Films of Adsorbed Nanospheres Studied by Quartz Crystal Microbalance (QCM). *Anal. Chem.* **2009**, *81*, 8167−8176.
(52) Vogt, B. D.; Lin, E. K.; Wu, W.-l.; White, C. C. Effect of Film Thickness on the Validity of the Sauerbrey Equation for Hydrated Polyelectrolyte Films. *J. Phys. Chem. B* **2004**, *108*, 12685−12690.
(53) van der Lee, A. Grazing incidence specular reflectivity: theory, experiment, and applications. *Solid State Sci.* **2000**, *2*, 257−278.
(54) Xie, K.; Fu, Q.; Webley, P. A.; Qiao, G. G. MOF Scaffold for a High-Performance Mixed-Matrix Membrane. *Angew. Chem., Int. Ed.* **2018**, *57*, 8597−8602.
(55) Prosser, J. H.; Brugarolas, T.; Lee, S.; Nolte, A. J.; Lee, D. Avoiding cracks in nanoparticle films. *Nano Lett.* **2012**, *12*, 5287−5291.
(56) Sanchez-Sanchez, M.; De Asua, I.; Ruano, D.; Diaz, K. Direct Synthesis, Structural Features, and Enhanced Catalytic Activity of the Basolite F300-like Semiamorphous Fe-BTC Framework. *Cryst. Growth Des.* **2015**, *15*, 4498−4506.
(57) Walcarius, A. Mesoporous materials and electrochemistry. *Chem. Soc. Rev.* **2013**, *42*, 4098.
(58) Walcarius, A. Mesoporous Materials-Based Electrochemical Sensors. *Electroanalysis* **2015**, *27*, 1303−1340.
(59) Walcarius, A. Silica-based electrochemical sensors and biosensors: Recent trends. *Current Opinion in Electrochemistry* **2018**, *10*, 88−97.
(60) Calvo, A.; Yameen, B.; Williams, F. J.; Soler-Illia, G. J.; Azzaroni, O. Mesoporous Films and Polymer Brushes Helping Each Other To Modulate Ionic Transport in Nanoconfined Environments. An Interesting Example of Synergism in Functional Hybrid Assemblies. *J. Am. Chem. Soc.* **2009**, *131*, 10866−10868.
(61) Calvo, A.; Yameen, B.; Williams, F. J.; Azzaroni, O.; Soler-Illia, G. J. A. A. Facile molecular design of hybrid functional assemblies with controllable transport properties: mesoporous films meet polyelectrolyte brushes. *Chem. Commun.* **2009**, 2553.

https://doi.org/10.1021/acs.jpcc.1c10425
J. Phys. Chem. C 2022, 126, 6724−6735

(62) Otal, E. H.; Angelomé, P. C.; Bilmes, S. A.; Soler-Illia, G. J. A. A. Functionalized Mesoporous Hybrid Thin Films as Selective Membranes. *Adv. Mater.* **2006**, *18*, 934−938.
(63) Velasco, M. I.; Acosta, R. H.; Marmisollé, W. A.; Azzaroni, O.; Rafti, M. Modulation of Hydrophilic/Hydrophobic Character of Porous Environments in Metal-Organic Frameworks via Direct Polymer Capping Probed by NMR Diffusion Measurements. *J. Phys. Chem. C* **2019**, *123*, 21076−21082.
(64) Weng, T.; Schmidt, J. R. Structure and Thermodynamic Stability of Zeolitic Imidazolate Framework Surfaces. *J. Phys. Chem. C* **2020**, *124*, 1458−1468.
(65) Cravillon, J.; Münzer, S.; Lohmeier, S.-J.; Feldhoff, A.; Huber, K.; Wiebcke, M. Rapid Room-Temperature Synthesis and Characterization of Nanocrystals of a Prototypical Zeolitic Imidazolate Framework. *Chem. Mater.* **2009**, *21*, 1410−1412.
(66) Tian, F.; Cerro, A. M.; Mosier, A. M.; Wayment-Steele, H. K.; Shine, R. S.; Park, A.; Webster, E. R.; Johnson, L. E.; Johal, M. S.; Benz, L. Surface and Stability Characterization of a Nanoporous ZIF-8 Thin Film. *J. Phys. Chem. C* **2014**, *118*, 14449−14456.
(67) Alberti, S.; Steinberg, P. Y.; Giménez, G.; Amenitsch, H.; Ybarra, G.; Azzaroni, O.; Angelomé, P. C.; Soler-Illia, G. J. A. A. Chemical Stability of Mesoporous Oxide Thin Film Electrodes under Electrochemical Cycling: from Dissolution to Stabilization. *Langmuir* **2019**, *35*, 6279−6287.
(68) Bindini, E.; Chehadi, Z.; Faustini, M.; Albouy, P.-A.; Grosso, D.; Cattoni, A.; Chanéac, C.; Azzaroni, O.; Sanchez, C.; Boissière, C. Following in Situ the Degradation of Mesoporous Silica in Biorelevant Conditions: At Last, a Good Comprehension of the Structure Influence. *ACS Appl. Mater. Interfaces* **2020**, *12*, 13598−13612.
(69) Muramatsu, H.; Tamiya, E.; Karube, I. Computation of equivalent circuit parameters of quartz crystals in contact with liquids and study of liquid properties. *Anal. Chem.* **1988**, *60*, 2142−2146.
(70) Martin, S. J.; Granstaff, V. E.; Frye, G. C. Characterization of a quartz crystal microbalance with simultaneous mass and liquid loading. *Anal. Chem.* **1991**, *63*, 2272−2281.
(71) Su, H.; Chong, S.; Thompson, M. Interfacial Hybridization of RNA Homopolymers Studied by Liquid Phase Acoustic Network Analysis. *Langmuir* **1996**, *12*, 2247−2255.
(72) Bélanger, S.; Stevenson, K. J.; Mudakha, S. A.; Hupp, J. T. Perfect" Electrochemical Molecular Sieving by Thin and Ultrathin Metallopolymeric Films. *Langmuir* **1999**, *15*, 837−843.
(73) Guo, J.; Lindner, E. Cyclic Voltammograms at Coplanar and Shallow Recessed Microdisk Electrode Arrays: Guidelines for Design and Experiment. *Anal. Chem.* **2009**, *81*, 130−138.
(74) Peerce, P. J.; Bard, A. J. Polymer films on electrodes. Part II. Film structure and mechanism of electron transfer with electrodeposited poly(vinylferrocene). *J. Electroanal. Chem.* **1980**, *112*, 97−115.
(75) Leddy, J.; Bard, A. J. Polymer films on electrodes. Part XII. Chronoamperometric and rotating disk electrode determination of the mechanism of mass transport through poly(vinyl ferrocene) films. *J. Electroanal. Chem.* **1983**, *153*, 223−242.
(76) Zhu, M.; Lerum, M. Z.; Chen, W. How to prepare reproducible, homogeneous, and hydrolytically stable aminosilane-derived layers on silica. *Langmuir* **2012**, *28*, 416−423.
(77) Mokrani, C.; Fatisson, J.; Guérente, L.; Labbé, P. Structural Characterization of (3-Mercaptopropyl)sulfonate Monolayer on Gold Surfaces. *Langmuir* **2005**, *21*, 4400−4409.

https://doi.org/10.1021/acs.jpcc.1c10425
J. Phys. Chem. C 2022, 126, 6724−6735